Study of NiFe/Al/Al_2O_3 magnetic tunnel junction interfaces using second-harmonic magneto-optic Kerr effect

S. E. Russek, T. M. Crawford, and T. J. Silva
Electromagnetic Technology Division, National Institute of Standards and Technology, Boulder, Colorado 80303

Using the second-harmonic magneto-optic Kerr effect (SHMOKE), we have measured the interfacial magnetic properties of NiFe/Al/Al_2O_3 heterostructures as a function of Al_2O_3 thickness and processing conditions. The samples were prepared like magnetic tunnel junctions except that the top electrodes were not deposited. A large change in SHMOKE contrast was observed for different oxidation processes and Al_2O_3 thicknesses. The magnetic SHMOKE contrast from a plasma oxidized sample in which the oxidation front is thought to be inside the original NiFe film is 70%, whereas the SHMOKE contrast from a thermally oxidized NiFe/Al sample, in which the oxidation front is ~1 nm from the Al/NiFe interface is only 15%. Further, the phase of the signal is reversed between the two structures. The SHMOKE data have been correlated with tunneling measurements on similarly fabricated structures. For the two samples listed above, the junction resistivity varied from $10^{-1}\,\Omega\,\mathrm{cm}^2$ (plasma oxidized) to $10^{-6}\,\Omega\,\mathrm{cm}^2$ (thermally oxidized). These results indicate that SHMOKE may be useful for assessing tunnel junction quality during processing.
[S0021-8979(99)49408-3]

I. INTRODUCTION

Recent advances in magnetic tunnel junction (MTJ) performance have made them strong candidates for use as magnetic data storage elements and magnetic sensors.[1,2] The resistance change of MTJs, as the magnetizations of the layers change from an antiparallel to a parallel state, is a strong function of the electronic and magnetic structure at the magnetic–insulator interface.[3,4] The electronic and magnetic structure at the interfaces is dependent on the junction fabrication process which can introduce mixing of the magnetic and nonmagnetic layers, leave residual nonmagnetic material at the interface, or introduce magnetic oxides at the interface. A promising new technique to measure the electronic and magnetic structure at these buried interfaces is to look at second-harmonic optical generation in response to ultrafast optical pulses.[5–8] Second-harmonic generation occurs at interfaces where the inversion symmetry of the electronic potentials and electron density is broken. The magnetization-dependent part of the second harmonic signal arises from the first few magnetic atomic layers that are in proximity to nonsymmetric potentials.

In this article we use the second-harmonic magneto-optical Kerr effect (SHMOKE) to investigate the electronic and magnetic properties at buried NiFe–Al–Al_2O_3 interfaces. We found that the SHMOKE signal varied considerably with oxidation time and oxidation process. In the early stages of Al oxidation, the SHMOKE contrast was out of phase with air-exposed NiFe (Ref. 9) and its magnitude increased as the oxidation depth increased. With further oxidation the SHMOKE contrast displayed a negative maximum and a subsequent sign change.

Magnetic tunnel junctions were fabricated under several different oxidation conditions, and the SHMOKE data provided a rapid method of characterizing the tunnel junction barriers and comparing different oxidation processes to quickly identify optimum processing conditions.

II. EXPERIMENT AND RESULTS

Magnetic thin-film structures were fabricated by sputter deposition onto oxidized Si substrates. The structures for the SHMOKE studies consisted of 10 nm Ta/ 50 nm $Ni_{80}Fe_{20}$/ 2.5 nm Al. The Al layers were oxidized by three different processes: thermal oxidation (exposure to air), oxidation by a remotely generated oxygen plasma with various substrate bias voltages, and oxidation by a local plasma generated by the substrate stage bias voltage. The SHMOKE data were taken *ex situ* after exposure to air for several hours. The plasma oxidized samples were stable (gave reproducible SHMOKE response) for several weeks after fabrication and the thermally oxidized samples were stable after 12 h of air exposure.

The SHMOKE apparatus is described in detail in Ref. 9. A mode-locked Ti-sapphire laser produces 50 fs pulses at a wavelength of 800 nm. The second-harmonic light, at a wavelength of 400 nm, is detected as a function of applied field in a *p*-transverse geometry (*p*-polarized incident light, magnetization transverse to the plane of incidence). The spot size is approximately 30 μm, and the peak intensities exceed 30 $\mathrm{GW/cm}^2$.

Additional samples were made in an identical manner to the SHMOKE samples except that top magnetic layers and pinning layers were deposited. Tunnel junction structures were patterned using a four-step lithographic process. Figure 1 shows the magnetoresistive response for a 10 μm×20 μm MTJ for 10 μA and 100 μA bias currents.

Easy-axis SHMOKE hysteresis loops [second-harmonic (SH) intensity versus applied field] for thermally oxidized and local plasma-oxidized samples are shown in Fig. 2. These loops represent the two extremes of the oxidation processes investigated. The thermal oxidation process (12 h in

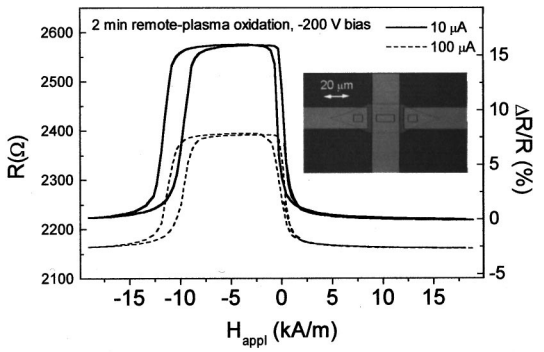

FIG. 1. Resistance as a function of applied field for a NiFe–Al_2O_3–NiFe 10 μm×20 μm magnetic tunnel junction for bias currents of 10 and 100 μA. The barrier was oxidized for 2 min in 6.7 Pa O_2 with a bias voltage of −200 V. The inset shows a micrograph of the device.

air) yields tunnel junctions with junction resistances of $10^{-6}\,\Omega\,\mathrm{cm}^2$ whereas the local-plasma oxidized process (12.0 Pa O_2, −400 V bias for 1 min) yields junctions with $10^{-1}\,\Omega\,\mathrm{cm}^2$. There is a substantial change in the SHMOKE contrast (the difference in second-harmonic intensities at positive and negative saturation normalized to the sum of the SH intensities) as well as a phase change in the SHMOKE response. The phase of the loop in Fig. 2(b) is identical to the phase seen in air-exposed NiFe.

To further investigate the region between these two extremes, hard-axis SHMOKE hysteresis loops were acquired as a function of oxidation time. The loops shown in Fig. 3 are for 2, 8, and 16 min remote plasma-oxidized samples with substrate biased at −200 V, which represent the range of behavior observable between the extremes shown in Fig. 2. The loop in Fig. 3(c) is inverted compared with the loop in Fig. 3(a), whereas the loop in Fig. 3(b) displays a very different behavior as a function of field than the other two loops.

The loop shapes observed in Fig. 3 were modeled using effective second-order susceptibility tensor elements for the

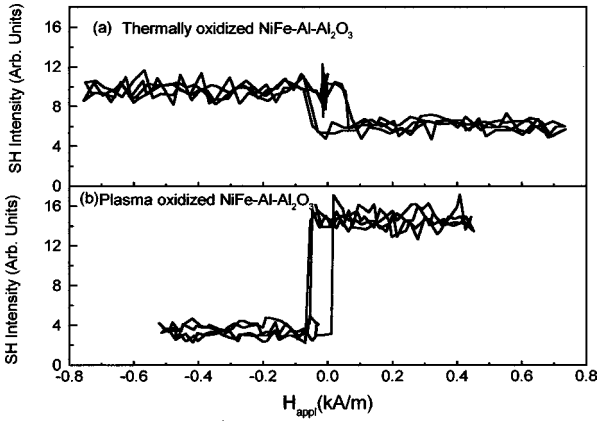

FIG. 2. (a) Easy axis SHMOKE hysteresis loop for a thermally oxidized NiFe–Al–Al_2O_3 structure. (b) Easy axis loop for a local plasma oxidized NiFe–Al–Al_2O_3 structure. Note that the contrast is 15% for the thermally oxidized sample and 70% for the plasma oxidized sample, and that the loop shape is inverted between the two.

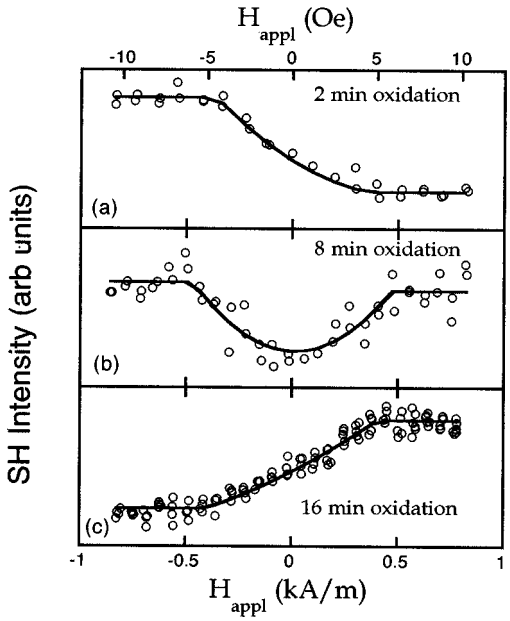

FIG. 3. (a) Hard axis SHMOKE hysteresis loop for 2 min remote plasma oxidized NiFe–Al–Al_2O_3 structure. (b) Same as (a), but for 8 min plasma oxidation. (c) Same as (a), (b) but for 16 min plasma oxidation. Note that the absence of a strong linear magnetization component in (b) allows the quadratic component to be clearly distinguished.

heterostructure. The SH intensity of a *p*-transverse SHMOKE measurement is

$$I_{\mathrm{SH}} \propto |\chi_{\mathrm{odd}} + \chi_{\mathrm{even}}|^2 \propto |\chi_{\mathrm{odd}}|^2 + |\chi_{\mathrm{even}}|^2 + 2\cos(\phi) \cdot \chi_{\mathrm{even}} \cdot \chi_{\mathrm{odd}}, \quad (1)$$

where χ_{odd} is assumed to be linear in **M**, and χ_{even} is even in or independent of **M**.[10] ϕ represents the phase difference between the even and odd tensor elements. In Ref. 10, it was shown that χ_{odd} was linear in magnetization angle (linear in applied field H_t for coherent rotation), and thus Eq. (1) predicts that there should be a SH contribution to the hysteresis loop which is quadratic in applied field for large values of χ_{odd} relative to χ_{even}. Therefore, Eq. (1) predicts a hysteresis loop which contains three primary components: independent of H_t, linear in H_t, and quadratic in H_t (for $H_t < H_k$, where H_k is the uniaxial anisotropy field). Contributions which scale as M^4 and higher were not included in the model. A modified version of Eq. (1) was used to fit the loops in Fig. 3 and obtain the ratio of odd to even tensor elements,

$$I_{\mathrm{SH}} = A\left[1 + 2\cos(\phi)\cdot\left|\frac{\chi_{\mathrm{odd}}}{\chi_{\mathrm{even}}}\right|\left(\frac{H_t}{H_k}\right) + \left|\frac{\chi_{\mathrm{odd}}}{\chi_{\mathrm{even}}}\right|^2\left(\frac{H_t}{H_k}\right)^2\right], \quad (2)$$

where H_k, ϕ, and $\chi_{\mathrm{odd}}/\chi_{\mathrm{even}}$ are fitting parameters, and A is a scaling parameter. For Fig. 3(a), we obtain $H_k = 360 \pm 80$ A/m (4.5±1 Oe), $\phi = 130° \pm 17°$, and $\chi_{\mathrm{odd}}/\chi_{\mathrm{even}} = 0.46 \pm 0.1$. For Fig. 3(b), we obtain $H_k = 464 \pm 240$ A/m (6±3 Oe), $\phi = 90.5° \pm 3°$, and $\chi_{\mathrm{odd}}/\chi_{\mathrm{even}} = 0.32 \pm 0.1$, while Fig. 3(c) yields $H_k = 400 \pm 40$ A/m (5±1 Oe), $\phi = 47° \pm 6°$, and $\chi_{\mathrm{odd}}/\chi_{\mathrm{even}} = 0.24 \pm 0.05$. The primary magnetization-dependent component in Fig. 3(b) is the quadratic piece aris-

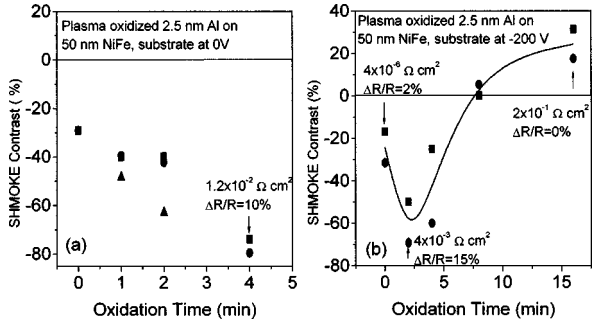

FIG. 4. (a) SHMOKE amplitude vs oxidation time for remote-plasma oxidized samples with stage potential held at ground. The circles and squares are the same set of samples measured on different days to indicate the stability of the measurements. The triangles represent a different set of samples oxidized in the same manner. (b) SHMOKE amplitude vs oxidation time for remote-plasma oxidized samples with the stage potential held at −200 V.

ing from χ_{odd}. The linear contribution is weak because ϕ is close to 90°, not because χ_{odd} is going to zero.

The SHMOKE contrast as a function of oxidation time, for two different oxidation processes, is shown in Fig. 4. Figure 4(a) shows the SHMOKE contrast for remotely generated plasma oxidation at a chamber pressure of 6.6 Pa O_2 with the substrate stage grounded. The SHMOKE contrast increases monotonically in the negative direction. Figure 4(b) shows the SHMOKE contrast for oxidation with the same conditions, except that the substrate stage was biased at −200 V. The substrate bias causes the oxidation to proceed more quickly and the SHMOKE contrast exhibits a maximum in the negative direction for 2 min oxidation time and then decreases and crosses zero at 8 min. If the SHMOKE contrast is assumed to follow a universal curve similar to that shown in Fig. 4(b), then the rates of the different oxidation processes can be determined by scaling the SHMOKE data to a universal curve. Roughly, the relative rates for a remote plasma oxidation (6.6 Pa O_2, 0 V bias), remote plasma oxidation (13.3 Pa O_2, −200 V bias), and local plasma oxidation (13.3 Pa O_2, −400 V bias) are 1:2:16.

Magnetic tunnel junctions were fabricated at several different oxidation conditions, as shown by the arrows in Fig. 4. The junction resistivities and the magnetoresistance are also indicated in Fig. 4. The best junctions were made near the negative maximum of the SHMOKE response. The thermally oxidized junctions were made using a 12 h, 26.6 kPa O_2 exposure in the deposition chamber before deposition of the top electrode. The low value of the magnetoresistance can be attributed to a thick layer of unoxidized Al remaining in the junction. The local plasma-oxidized samples showed high resistances (typically 200 kΩ for a 10 μm×20 μm junction) and nonlinear current–voltage curves, but did not display any junction magnetoresistance, which is consistent with the oxidation front having passed into the magnetic layer.

III. DISCUSSION AND SUMMARY

As oxidation occurs, the oxidation front moves through the Al layer to the magnetic layer. The Al–Al_2O_3 interface is a strong second-harmonic generator which, when it is far from the magnetic layer, is magnetization independent. The Al–NiFe interface is a weaker source of SH generation; however, it has a magnetization-dependent component. When the oxidation front approaches and moves through the magnetic interface, the multilayer geometry rapidly changes composition, from NiFe–Al–Al_2O_3 to NiFe–NiFe–oxide–Al_2O_3. When the interface composition changes, large changes in the SHMOKE signal are expected. The model described by Eq. (1) combines the SH contributions from the two interfaces into a single effective SH intensity from a single interface.

This model provides significant information, even though the details of the optical propagation through the structure and the multiple interface SH contributions need to be considered. The phase between the tensor elements undergoes a large change, from ~130° to ~50°, passing near 90° for the 8 min oxidation time, allowing only the quadratic magnetization-dependent contribution to be observed [Fig. 3(b)]. These observations imply that we are observing a single magnetic interface which undergoes a significant change when the oxidation front passes through the NiFe boundary, rather than an interface interference effect, although interference effects cannot be ruled out without performing the more detailed multilayer model calculation for the SHMOKE response from this heterostructure.[9]

While the large phase change from Figs. 3(a) to 3(c) likely indicates the passing of the oxidation front through the NiFe boundary, more careful measurements as a function of oxidation time are required to correlate the SHMOKE response with the exact position of the oxidation front. However, even the current empirical correlation between the SHMOKE data and the MTJ properties proved useful in optimizing the tunnel barrier properties without having to microfabricate large numbers of tunnel junctions.

[1] J. S. Moodera, L. R. Kinder, T. M. Wong, and R. Meservey, Phys. Rev. Lett. **74**, 3273 (1995).
[2] W. J. Gallagher *et al.*, J. Appl. Phys. **81**, 3741 (1997).
[3] R. Jansen and J. S. Moodera, J. Appl. Phys. **83**, 6682 (1998).
[4] J. M. MacLaren, W. H. Butler, and X.-G. Zhang, J. Appl. Phys. **83**, 6521 (1998).
[5] R. Pin-Pan, H. D. Wei, and Y. R. Shen, Phys. Rev. B **39**, 1229 (1989).
[6] B. Koopmans, M. G. Koerkamp, and Th. Rasing, Phys. Rev. Lett. **74**, 3692 (1995).
[7] Q. Y. Jin, H. Regensburger, R. Vollmer, and J. Kirschner, Phys. Rev. Lett. **80**, 4056 (1998).
[8] K. J. Veenstra, P. E. Hansen, A. Kirilyuk, and Th. Rasing, J. Magn. Magn. Mater. (in press).
[9] T. M. Crawford, C. T. Rogers, T. J. Silva, and Y. K. Kim, Appl. Phys. Lett. **68**, 1573 (1996).
[10] T. M. Crawford, C. T. Rogers, T. J. Silva, and Y. K. Kim, IEEE Trans. Magn. **33**, 3598 (1997).